Progress In Electromagnetics Research M, Vol. 53, 167–175, 2017

A Portable Frequency Domain Electromagnetic System for Shallow Metal Targets Detection

Xiaodong Qu[1, 2, *], Yade Li[1, 2], Guangyou Fang[1], and Hejun Yin[1]

Abstract—In this paper, a portable frequency domain electromagnetic system CEM-2 is presented for shallow metal targets detection. This paper discusses the detection principle of frequency domain electromagnetic system, introduces hardware implementation, presents test results of each module, and gives the system's imaging results in field tests. Sinusoidal pulse width modulation technique is employed in this system to produce single-frequency or multi-frequencies synthetic electromagnetic signals with signal to noise ratio of about 85 dB. After integration, the CEM-2 system's in-phase noise level is about 90 ppm while the quadrature response is about 100 ppm. The experiment results of CEM-2 agree well with the simulation ones both from signatures and amplitudes. The experiment for detecting targets of different sizes and materials conducted in field indicates that CEM-2 system can be used to distinguish metallic and ferrous objects.

1. INTRODUCTION

Subsurface detection of underground objects such as communication cables, pipes and other public infrastructure has attracted considerable public attention. The unexploded ordnance buried underground in some areas is a continuous threat to people's life. The duds left during shooting training and live-fire exercises seriously restrict people's activities range. In recent years, due to its portability and efficiency, frequency domain electromagnetic system is widely used in the field, such as unexploded ordnance detection [1], shallow surface mapping [2] and archeology [3].

Unlike ground penetrating radar (GPR) which measures the electromagnetic wave reflected by boundary, frequency domain electromagnetic system [4] measures the secondary magnetic field generated by eddy current induced in the anomaly targets which are illuminated by alternating primary electromagnetic field. For GPR, the resolution and detection depth depend on the operation frequency. As the frequency increases, the resolution increases while the effective detection depth decreases. Thus, GPR only shows advantages to detect very shallow detection. Furthermore, when the soil contains much water, GPR can hardly penetrate through the soil to detect the targets. On the other hand, frequency domain electromagnetic system can achieve the detection depth. The resolution is determined by the coil geometry.

Currently, commercial products mainly include EM31-MK2, EM34-3, EM38 by Geonics [5, 6], GEM-2, GEM-3, GEM-5 by Geophex [7–9] and Russian NEMFIS [3] system. Based on geometric sounding principle, EM series systems made by Geonics can achieve different depth sounding by changing the distance between transmitter and receiver and the corresponding operating frequency. Thus, the operation is complex and inefficient. Alternatively, GEM Series systems, designed based on the frequency sounding principle by Geophex, can achieve different depth sounding by changing the operating frequency.

Received 16 November 2016, Accepted 9 January 2017, Scheduled 28 January 2017

* Corresponding author: Xiaodong Qu (dongdongqu@126.com).

[1] Key Laboratory of Electromagnetic Radiation and Sensing Technology, Institute of Electronics,Chinese Academy of Sciences, Beijing 100190, China. [2] University of Chinese Academy of Sciences, Beijing 100190, China.

In this paper, we study the key technologies and hardware circuits for portable frequency domain electromagnetic system and conducted experiments with the integrated system. CEM-2 employs three coplanar coils attached to a single support ski so that it can be operated by one person and for outside detection. Secondly, sinusoidal pulse width modulation (SPWM) technology is employed to generate arbitrary digital signal waveform whose total harmonic distortion (THD) is low. Thirdly, the convolution between signals and standard time series rends a narrow-band matched filter. By doing complex division, the normalized in-phase response and quadrature response can be obtained. Finally, the mounting positions of the metal items are selected according to the principle that primary magnetic field has minimum gradient.

2. SYSTEM DESIGN

Based on the law of electromagnetic induction, frequency domain electromagnetic system CEM-2 is designed. The transmitter generates single frequency or multi-frequencies synthesized primary signal, establishing harmonic primary field around the target. According to Lenz's law, eddy currents will be induced in anomaly target. The eddy current generates secondary electromagnetic field to hinder primary field's changes in turn. The targets' physical properties can be obtained from the secondary electromagnetic field. This paper presents a portable frequency domain electromagnetic system CEM-2 for shallow unexploded ordnance detection within less than 2 m, as shown in Fig. 1.

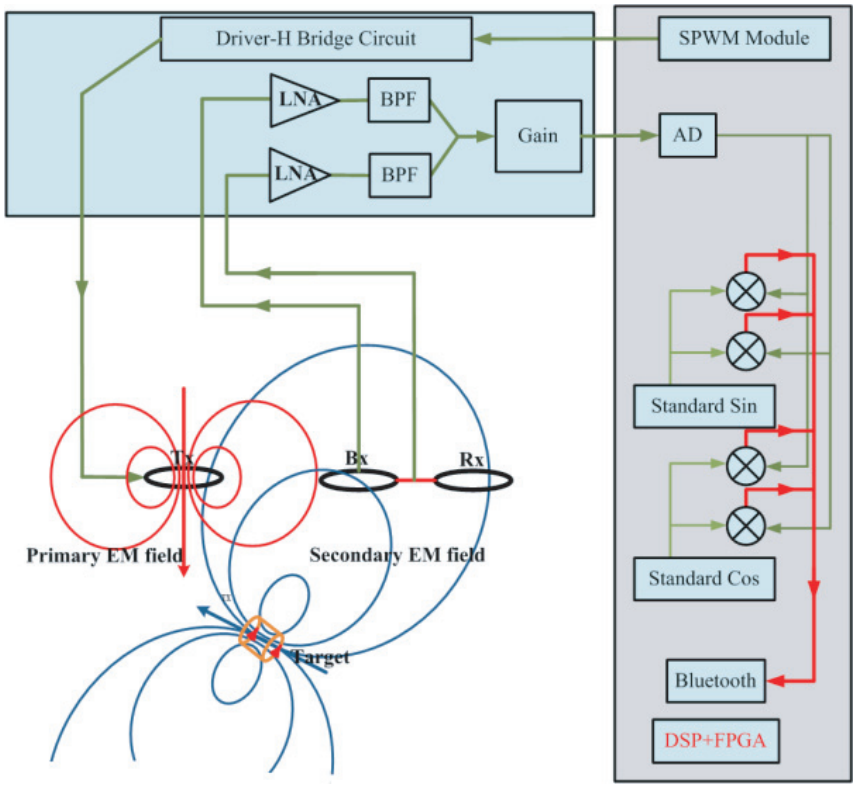

Figure 1. The block diagram of CEM-2 system.

2.1. Transmitter System

The transmitter system mainly contains DSP unit, driver circuit, H-bridge circuit and transmitter coil. The scheme diagram is shown in Fig. 2.

Technical methods that can produce multi-frequencies signal mainly include bitstream method [10] and pseudorandom method [11]. The bit stream method uses more complicated algorithm to generate

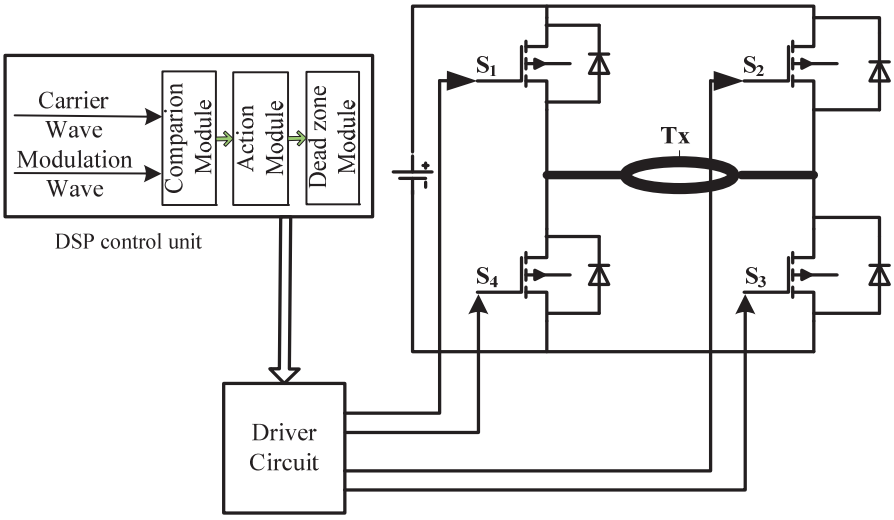

Figure 2. The scheme diagram of transmitter system.

multi-frequencies signals. The algorithm also depends on the load. The pseudorandom method can only generate multi-frequencies current signals with fixed frequency intervals. The total harmonic distortion of current signal is so large that power amplifier is required. To overcome the shortcomings of the existing techniques, CEM-2 employs SPWM technology [12] to generate arbitrary digital signal waveform which has low total harmonic distortion (THD).

When narrow pulses with equal impulse and different shapes are applied to the inertia components, the effects are almost the same. The SPWM technology employs irregular sampling method to produces quare pulses with adjustable duty cycle (switching signals), which is used to control CMOSs to produce the desired current waveform. The transmitter generates switching signals by DSP that contains carrier wave (triangular wave) and modulated wave (required current waveform) generation module, comparison module, action module, and dead zone module. Switching signals control H-bridge circuit which consists of four CMOSs through the drive circuit. The DC power (12 V, can be adjusted to meet the requirements for the magnetic moment) is supplied on the transmitter coil when S1&S3 (or S2&S4) are open, to achieve DC-AC inversion. The transmitter coil is an air coil with enameled wire wound on ABS. To meet the required magnetic moment, it is necessary to optimize the parameters of diameter, number of turns and way of winding. After optimization, the transmitter coil consists of four 100-turn coils in parallel. The physical parameters of transmitter coil are inductance $L = 3\,\text{mH}$, resistance $R = 1.765\,\Omega$, resonance frequency $fc = 55.45\,\text{kHz}$. The size of the transmitter coil is about $17 \times 12\,\text{cm}$. Some current waveforms and power spectrum densities (PSD) examples of various frequencies synthesized signals are shown in Fig. 3.

Figure 3(a) shows a single frequency current waveform and power spectrum density of transmitter current at 275 Hz. Fig. 3(b) shows current waveform and power spectrum density of transmitter current at 425 Hz and 1025 Hz. Fig. 3(c) shows current waveform and power spectrum density of transmitter current at 275 Hz, 425 Hz, 675 Hz, 1025 Hz and 2075 Hz. From the power spectrum density, the transmitter can generate the required current signals with low THD (1.88% @ 275 Hz) arbitrary frequency intervals and high signal to noise rate (about 85 dB).

2.2. Receiver System

Receiver system mainly consists of DSP/FPGA module, data acquisition module, data transmission module, and magnetic sensors module. The scheme diagram is shown in Fig. 4.

The CEM-2 system includes 2 channel receiver systems, collecting reference signal from reference coil and secondary signal from differential connection between receiver coil and reference coil. In order to satisfy the requirement for processing and displaying real-time during anomaly detection process, the

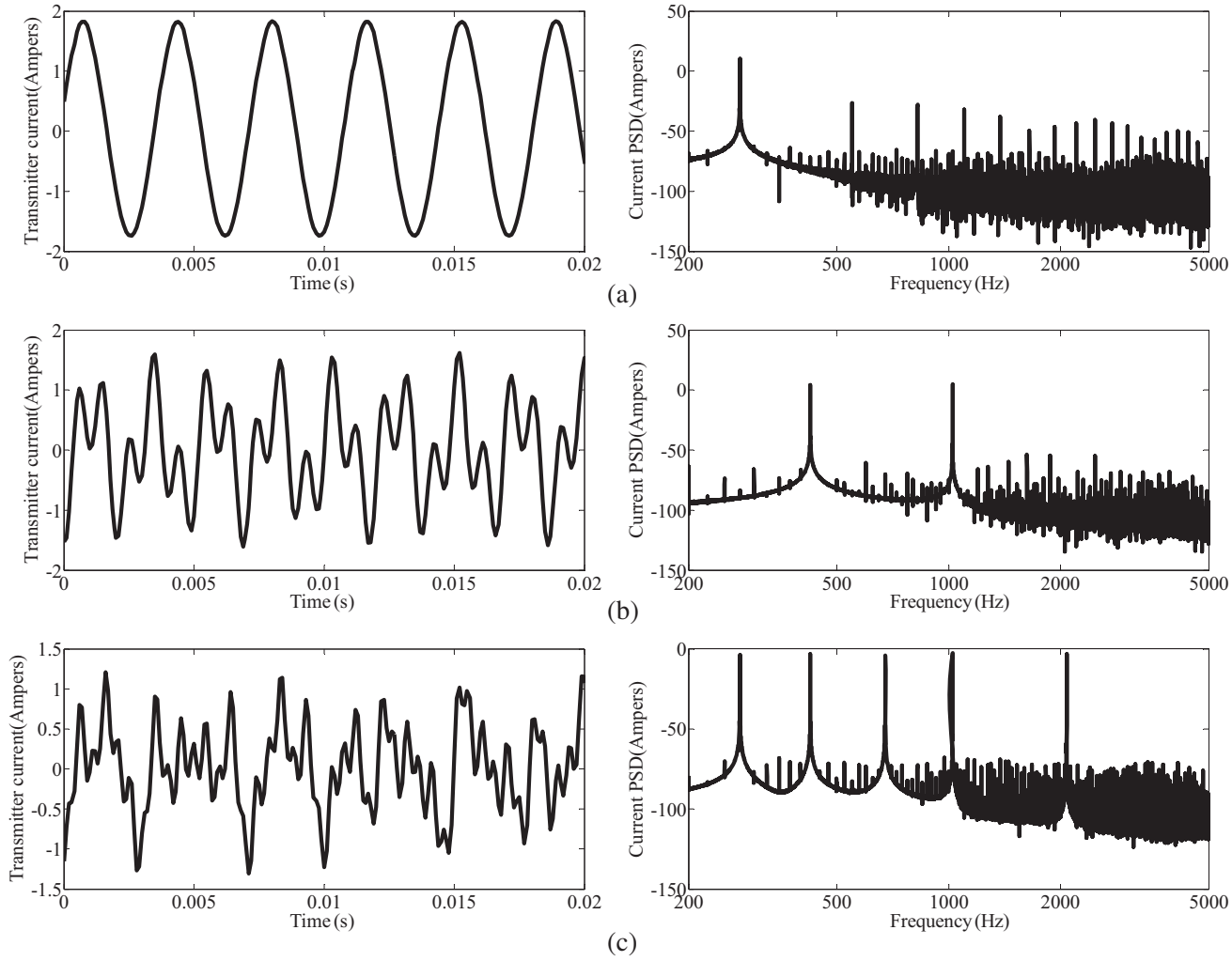

Figure 3. Results for transmitter current. (a) Single frequency current waveform and PSD. (b) Two frequencies synthetic current waveform and PSD. (c) Five frequencies synthetic current waveform and PSD.

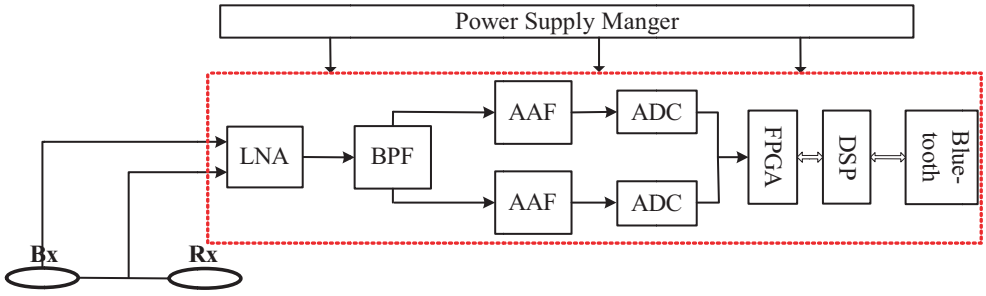

Figure 4. The scheme diagram of receiver system.

central control unit consists of FPGA timing control module and DSP data processing module. The unit which can ensure the right timing and real-time data processing controls the entire system. FPGA timing control module generates the correct time sequence for data acquisition module ensures time synchronization between the 2-channel receivers and caches the raw data into the internal FIFO. When the acquisition time reaches 1/25 s (power-frequency is 50 Hz), FPGA transfers the original data to DSP

via data bus and address bus. After data processing in DSP, the in-phase components and quadrature components extracted from the secondary field with respect to the primary field are transferred to PDA for real-time display and storage via Bluetooth.

Data acquisition module is the core of the receiver system. Eventually, 24-Bit, Sigma-Delta analog-digital converter (ADC) chips AD7763 are selected after comparison and screening. AD7763 made in Analog Devices works at a sampling rate of 78125 kHz. The dynamic range is approximately 120 dB. Bluetooth data transmission module using TI's CC254X chip conveys operating parameters and control instructions from operator and transfers the processed data to PDA for display and storage. PDA is used to achieve human-computer interactions

2.3. Magnetic Sensors

Magnetic sensor module consists of sensors module and signal conditioning module.

Sensors which are air induction coils convert magnetic field into voltage sampled by ADs. To achieve the requirements of sensitivity, gain and bandwidth, optimization of diameter and number of turns is necessary. Finally, parameters of receiver coil (Rx) are: number of turns $N = 400$, inductance $L = 43.38\,\text{mH}$, resistance $R = 25.6\,\Omega$, $fc = 76\,\text{kHz}$; parameters of reference coil (Bx) are: number of turns $N = 100$, inductance $L = 2.78\,\text{mH}$, resistance $R = 6.2\,\Omega$, $fc = 202\,\text{kHz}$.

Signal conditioning module includes low noise amplifiers, analog bandpass filters and single-ended signal to differential signal converters. According to Ferris formula, the noise level of the entire instrument system mainly depends on the noise level of the preamplifier. After comparing bandwidth, input impedance and equivalent input voltage noise of different amplifiers, INA163 which is a low noise instrumentation differential amplifier is eventually selected eventually as preamplifier. The magnification is about 267 times according to the test results. Analog bandpass active filter is designed in a Sallen-Key structure, and the bandwidth is 200 Hz $\sim$ 20 kHz. The amplifier AD8021 is used to invert the single-ended signal to differential signal. Amplitude frequency characteristic of signal conditioning module is shown in Fig. 5. The amplitude frequency characteristics of two channels coincide well with good flatness. The noise performance of the signal conditioning module is measured with a terminated input. The power density of the equivalent input noise is about $1.33\,\text{nv}/\sqrt{\text{Hz}}$ as shown in Fig. 6.

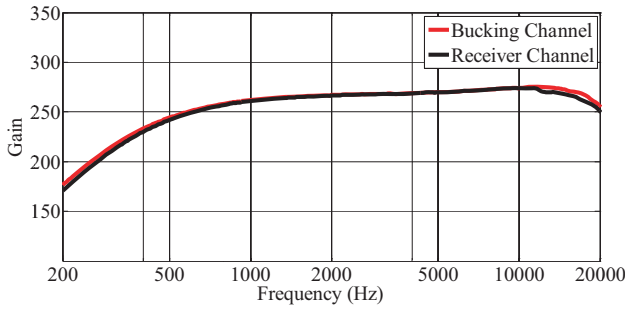

Figure 5. Amplitude frequency characteristic.

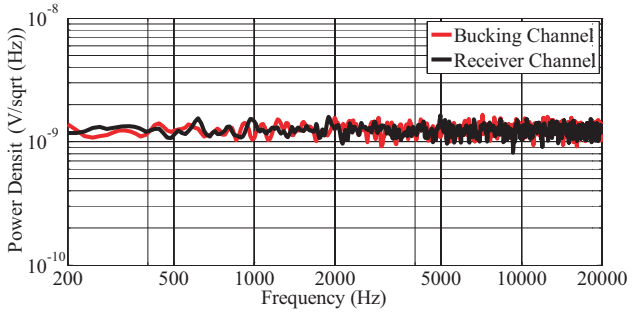

Figure 6. Power density of equivalent input noise.

2.4. Integrated Instrument System

The integrated portable frequency domain electromagnetic system for shallow unexploded ordnance detection is shown in Fig. 7. All the magnetic sensors (Tx, Bx and Rx) and circuits are placed on a ski wood. The receiver and transmitter are integrated in a removed box (RB) which is 0.62 m from the center of the transmitter coil. The signal conditioning circuits (SCC) are placed 1.3 m from the center of the transmitter coil. The mounting positions are selected according to the principle that primary magnetic field has minimum gradient.

The output noise performance of in-phase response and quadrature response is measured under a stable environment where few objects (cars and animals) approached the test site during the experiment. Environment noise keeps unchanged or changes very slowly. Also, the test site is far away from human

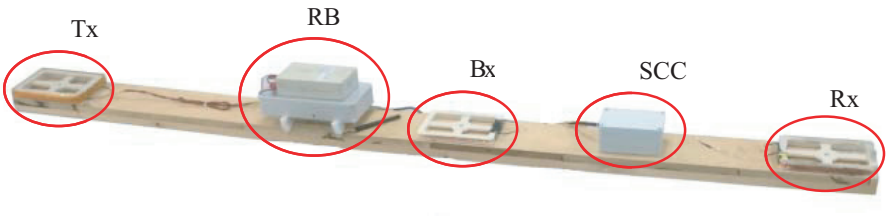

Figure 7. The integrated instrument system.

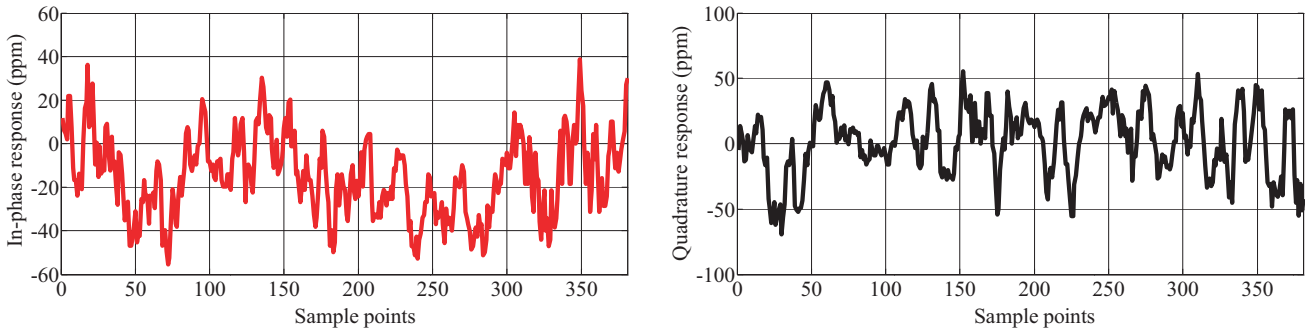

Figure 8. Output noise performance. (a) In-phase noise. (b) Quadrature noise.

beings to reduce cultural electromagnetic noise. Test results at 1025 Hz are shown in Fig. 8. It is clear that the noise level of in-phase response is about 90 ppm (peak-to-peak) while the quadrature response is about 100 ppm.

3. SIMULATION AND EXPERIMENTAL EXAMPLES

3.1. Comparison between Simulation and Experiment Results

To better display the consistency between the simulation results and measurement, a test coil with known parameters $r = 455.4\,\Omega$, $L = 217.5$ mH was used both in simulation models and experiment. The measurement was taken point by point. There were 15 measurement points in total. The measurement scenario is shown in Fig. 9. The magnetic moment is $3\,\mathrm{Am}^2$, and the operation frequency is 475 Hz.

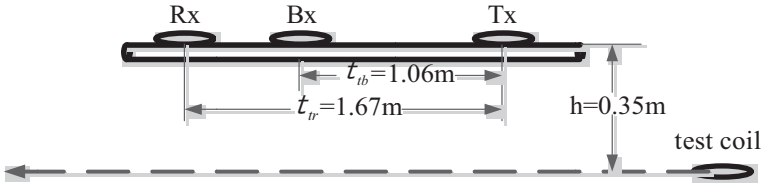

Figure 9. Simulation and experiment scenario.

Figure 10 shows the simulation and experiment results. In Fig. 10, the simulation results are shown in dashed lines while the experiment results are shown in dots. It is clear that the signatures of in-phase and quadrature response are consistent with the simulation results both in amplitude and signal shape. However, some deviations exist between the simulation and experiment results. The peak-to-peak amplitudes of the experiment results are a litter smaller than the simulation ones. Firstly, the position of Bx coil was not known exactly, which has great effects on the simulation results. Secondly, the position of the test coil in the experiment was not placed along the line used in the simulation exactly. Finally, the distributed capacitance of the test coil is not taken into consideration.

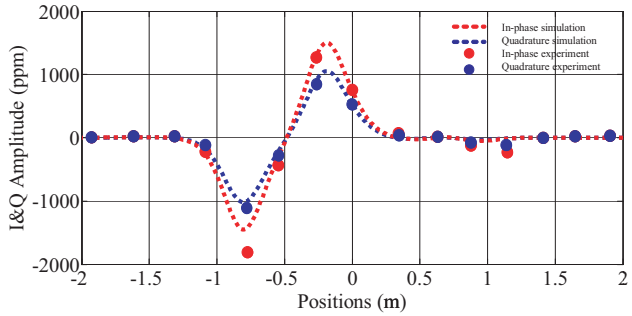

Figure 10. The comparison between simulation and experiment results.

3.2. Field Experiment

To test the CEM-2 system performance, an experiment was conducted in a test site. As shown in Fig. 11, 6 metallic targets of varied sizes and materials are buried about 20 cm underground in a 5 m $*$ 5.2 m experiment test site. The sizes of all the targets are not in proportion to the survey area, and the target T1 is vertical for diagrammatic drawing. The locations and descriptions of the targets are also shown. The CEM-2 system was operated by a single person, keeping horizontal at a height about 80 cm from the ground.

Target ID	Description	X(m)	Y(m)
P1	OD(8) $\times$ 35 cm steel horizontal, S-N	1	1
P2	OD(10) $\times$ 56 cm steel 35°, S(up)-N	2	4.3
P3	OD(2) $\times$ 8 cm steel horizontal, S-N	3	1.2
P4	OD(1.2) $\times$ 6 cm steel horizontal, E-W	4	4.5
L1	22.3 $\times$ 14.5cm aluminum sheet 12°, ES(up)-WN	5	1.2
T1	OD(10) $\times$ 20 cm ferromagnetic vertical	5	4.5

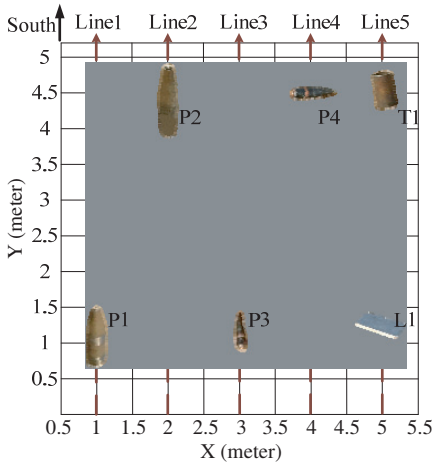

Figure 11. Target description under detection and experiment test site.

The experiment data at 475 Hz were collected along lines separated at interval of 1 m. Both the line profiles and area maps of in-phase and quadrature response are demonstrated in Fig. 12. We note that:

(1) Figures 12(a) and 12(c) show in-phase response of CEM-2 extracted from the secondary field. Four targets can be distinguished, shown using red oval logo. There are two main reasons that the target P4 is failed to be detected. Firstly, the outer diameter of P4 is about 1.2 cm and 6 cm in length. So, only weak eddy current can be induced in P4. Secondly, P4's major axis is perpendicular to the system, and this distribution reduces the response furthermore. As a result, the secondary field is difficult to be distinguished from the ambient noise. The target L1 cannot be seen in the in-phase response map. This is because the in-phase response is mainly proportional to the relative permeability while L1 is made up of aluminum whose relative permeability is about 1.

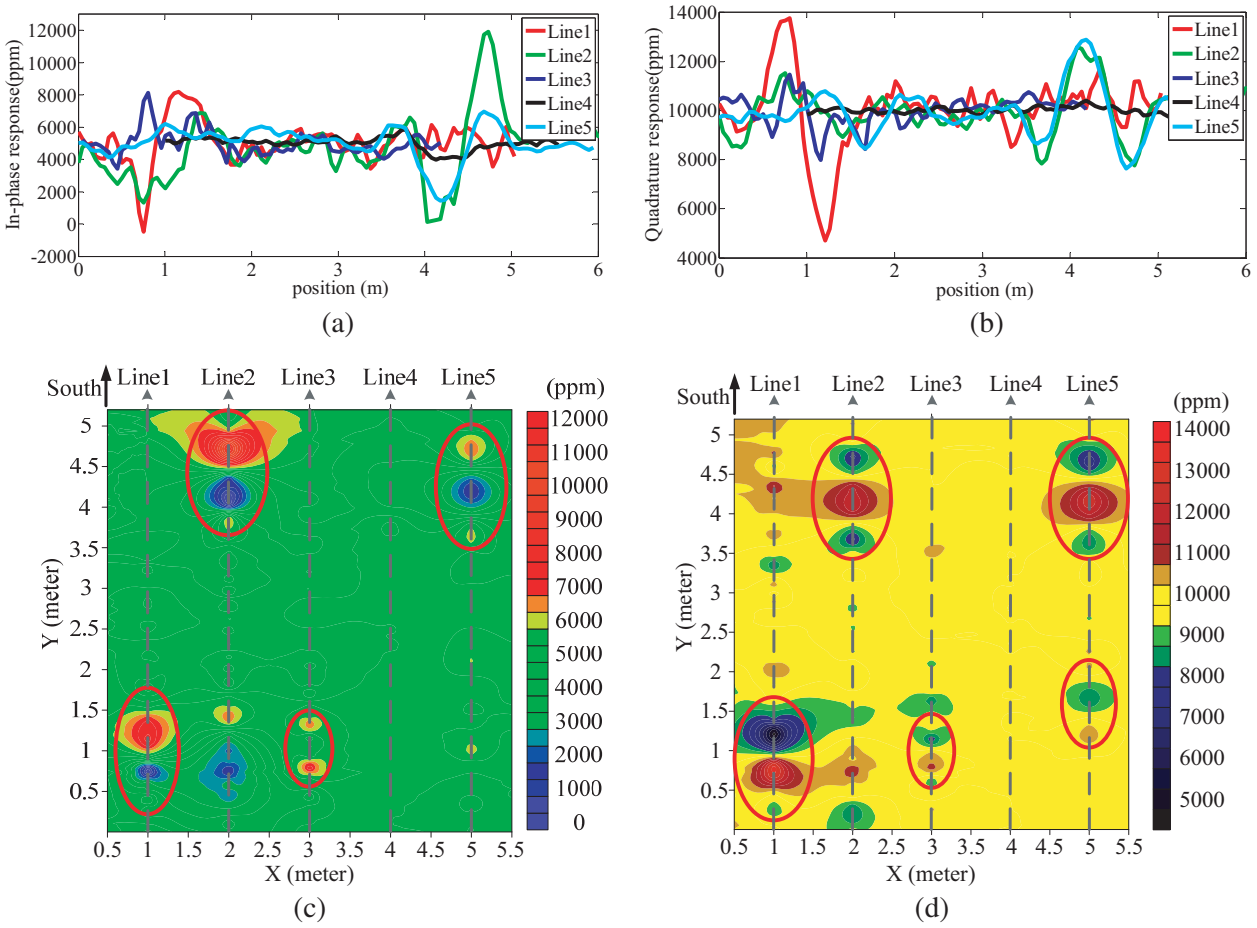

Figure 12. Experiment results for CEM-2. (a) In-phase profiles of the experiment data. (b) Quadrature profiles of the experiment data. (c) In-phase response map. (d) Quadrature response map.

(2) Figures 12(b) and 12(d) show the quadrature response of CEM-2 extracted from the secondary field. There are five targets that can be distinguished and shown with red oval logo. The target P4 is not detectable for the same reason as that of in-phase response. The target L1 can be detected in the quadrature response map because the quadrature response is mainly proportional to the electrical conductivity. Therefore, metallic objects can be distinguished from background by quadrature response while in-phase response is sensitive to magnetic objects.

However, there exist some false alarms in the in-phase response and quadrature response. The main reason is that the eddy current induced by a big target has large footprint which covers near area. For example, CEM-2 can detect P1 when surveying along Line 2. The method to reduce the false alarms is to refine the area and do detailed detection to confirm one or more targets.

4. CONCLUSION

This paper presents a portable frequency domain electromagnetic system CEM-2 for shallow detection. We have studied the key technologies, designed circuits and given test results for each module. Finally, noise performance and experimental results of the integrated CEM-2 system are discussed. It can be concluded that metallic objects with high conductivity and low relative permeability can be distinguished from background by quadrature response while magnetic and ferrous objects can be distinguished by in-phase response.

ACKNOWLEDGMENT

This work was supported by the National Natural Science Foundation of China under contract No. 41504064.

REFERENCES

1. Nelson, H. H. and D. A. Steinhurst, "Enhanced UXO discrimination using frequency-domain electromagnetic induction," ResearchGate, Jul. 2007.
2. Sharma, S. P., K. Anbarasu, S. Gupta, et al., "Integrated very low-frequency EM, electrical resistivity, and geological studies on the LantaKhola landslide, North Sikkim, India," *Landslides*, Vol. 7, No. 7, 43–53, Feb. 2010.
3. Manstein, Y. and A. Manstein, "EMI sensor NEMFIS: Method, equipment and case stories of archaeological prospection," *Archéosciences*, Vol. 33, No. 1, 321–324, Oct. 2009.
4. Zhdanov, M. S., "Electromagnetic methods in the frequency and time domains," *Methods in Geochemistry & Geophysics*, 649–693, Dec. 2009.
5. McNeill, J. D., "Electromagnetic terrain conductivity measurement at low induction numbers," *Geonics Ltd, Technical Note TN-6*, 1980.
6. McNeill, J. D., "Archaeological mapping using the Geonics EM38B to map Terrain Magnetic Susceptibility," *Geonics Ltd, Technical Note TN-35*, 2013.
7. Won, I. J., D. A. Keiswetter, G. R. A. Fields, et al., "GEM-2: A new multi-frequency electromagnetic sensor," *Journal of Environmental & Engineering Geophysics*, Vol. 1, No. 1, 129–138, Aug. 1996.
8. Won, I. J., D. A. Keiswetter, D. R. Hanson, et al., "GEM-3: A monostatic broadband electromagnetic induction sensor," *Journal of Environmental & Engineering Geophysics*, Vol. 2, No. 1, 53–64, Mar. 1997.
9. Huang, H., B. Sanfilipo, and I. J. Won, "Planetary exploration using a small electromagnetic sensor," *IEEE Transactions on Geoscience & Remote Sensing*, Vol. 43, No. 7, 1499–1506, Aug. 2005.
10. Bradshaw, J., U. Madawala, and N. Patel, "Techniques for conditioning bit-stream signals for single-phase power electronics applications," *IEEE Transactions on Power Electronics*, Vol. 27, No. 3, 1414–1423, Mar. 2012.
11. Gommé, L., G. Vandersteen, and Y. Rolain, "A high-speed on-chip pseudo-random binary sequence generator for multi-tone phase calibration," *Measurement Science & Technology*, Vol. 22, No. 7, 75901–75914, Jul. 2011.
12. Renge, M., H. Suryawanshi, and M. Chaudhari, "Digitally implemented novel technique to approach natural sampling SPWM," *EPE Journal*, Vol. 20, No. 1, 13–20, Jan. 2010.